Speed Sensorless Field-Orientation Control of the Induction Machine

Hirokazu Tajima and Yoichi Hori, *Member, IEEE*

Abstract— **We propose a speed estimation method for an induction machine and its application to the flux observer-based field-orientation (FOFO) control system, which we proposed previously. The motor speed is estimated based on the difference between two flux estimators. We analyze its convergence performance and propose the novel pole assignment method. Next, we apply this speed estimator to the FOFO controller. We implement the system centered about the DSP, and through some laboratory experiments, we will show that the speed sensorless FOFO operates with enough stability and has a strong robustness to rotor resistance variation.**

I. Introduction

WE KNOW TWO major techniques for high-performance control of induction machines: 1) slip frequency controlled type vector control and 2) field-orientation control.

Recently, the elimination of the speed sensor has been one of the important requirements in vector control systems because the speed sensor spoils the ruggedness and simplicity of ac motors. We can see some excellent speed sensorless approaches (for example in [2]), but they are applicable only to slip frequency-controlled-type systems.

In this paper, we will propose the speed sensorless control method applicable to field-orientation control. It is well known that field-orientation control is inherently more insensitive to rotor resistance variation than the slip frequency controlled system [5]. However, since the field-orientation controller has no concept of frequency, we should estimate the rotor speed from the instantaneous values of stator voltages and currents.

First, we refer to the speed estimation method proposed by Shauder [1] based on the idea of the model reference adaptive system (MRAS) and propose its novel pole allocation method. The estimated speed is instantaneously used for the flux observer-based field-orientation (FOFO) controller which we proposed some years ago [5]. Through the implementation using a digital signal processor (DSP) and some laboratory experiments, we will show that the speed-sensorless FOFO operates with enough stability and has strong robustness to changes in machine parameters such as the rotor resistance.

Paper IPCSD 92-4, approved by the Industrial Drives Committee of the Industry Applications Society for presentation of the 1991 Industry Applications Society Annual Meeting, Dearborn, MI, Sept. 28–Oct. 4. Manuscript released for publication Feb. 23, 1992.

The authors are with the Department of Electrical Engineering, University of Tokyo, Tokyo, Japan.

IEEE Log Number 9204180.

II. Model of Induction Machine

The state equation of the induction machines are given by

$$\dot{\boldsymbol{x}} = \begin{bmatrix} \boldsymbol{A}_{11} & \boldsymbol{A}_{12} \\ \boldsymbol{A}_{21} & \boldsymbol{A}_{22} \end{bmatrix} \boldsymbol{x} + \begin{bmatrix} \boldsymbol{B}_1 \\ o \end{bmatrix} \boldsymbol{v}_s \tag{1}$$

where

$$x = [\boldsymbol{i}_s, \boldsymbol{\lambda}_r]^T$$

$$\boldsymbol{A}_{11} = -\left(\frac{R_s}{\sigma L_s} + \frac{1-\sigma}{\sigma \tau_r}\right) \boldsymbol{I}$$

$$\boldsymbol{A}_{12} = \kappa\left(\frac{1}{\tau_r}\boldsymbol{1} - \omega_r \boldsymbol{J}\right) \qquad \boldsymbol{A}_{21} = \frac{M}{\tau_r}\boldsymbol{I}$$

$$\boldsymbol{A}_{22} = -\frac{1}{\tau_r}\boldsymbol{I} + \omega_r \boldsymbol{J} \qquad \boldsymbol{B}_1 = \frac{1}{\sigma L_s}\boldsymbol{I}$$

$$\sigma = 1 - \frac{M^2}{L_s L_r} \qquad \tau_r = \frac{L_r}{R_r} \qquad \kappa = \frac{M}{\sigma L_s L_r}$$

$$\boldsymbol{I} = \begin{bmatrix} 1 & 0 \\ 0 & 1 \end{bmatrix} \qquad \boldsymbol{J} = \begin{bmatrix} 0 & -1 \\ 1 & 0 \end{bmatrix}.$$

The state variables are the stator current $\boldsymbol{i}_s = (i_{sa}, i_{sb})^T$ and the rotor flux $\boldsymbol{\lambda}_r = (\lambda_{ra}, \lambda_{rb})^T$. The input variable is the stator voltage $\boldsymbol{v}_s = (v_{sa}, v_{sb})^T$. Note that all variables are handled on the stator coordinate system.

III. Speed Estimator

A. Configuration of Speed Estimator

From (1), we can obtain two well-known flux simulators. One is called the voltage model, and the other is called the current model.

Voltage Model:

$$\dot{\hat{\boldsymbol{\lambda}}}_{rv} = \frac{L_r}{M}(\boldsymbol{v}_s - R_s \boldsymbol{i}_s - \sigma L_s \dot{\boldsymbol{i}}_s). \tag{2}$$

Current Model:

$$\dot{\hat{\boldsymbol{\lambda}}}_{ri} = \left(-\frac{1}{\tau_r}\boldsymbol{I} + \omega_r \boldsymbol{J}\right)\hat{\boldsymbol{\lambda}}_{ri} + \frac{M}{\tau_r}\boldsymbol{i}_s. \tag{3}$$

The voltage model of (2) does not involve rotor speed ω_r, whereas the current model of (3) does. We can then estimate the speed based on the output difference between these two models.

$$\hat{\omega}_r = \left(K_P + \frac{K_I}{s}\right)\epsilon \tag{4}$$

where

$$\epsilon = \hat{\lambda}_{ria}\hat{\lambda}_{rvb} - \hat{\lambda}_{rva}\hat{\lambda}_{rib}. \tag{5}$$

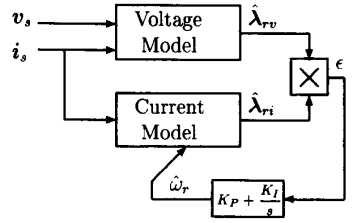

Fig. 1. Configuration of the speed estimator.

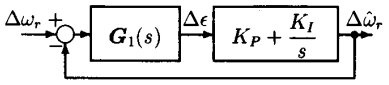

Fig. 2. Speed estimator dynamics.

The adaptive mechanism of (5) is derived from using Popov's criterion for hyperstability [1]. Fig. 1 illustrates this idea of speed estimation.

Through the linearization with respect to a certain operating point, we can obtain the transfer function from the estimation error $\Delta\omega_r - \Delta\hat{\omega}_r$ to $\Delta\epsilon$ as follows [1]:

$$G_1(s) = \frac{\Delta\epsilon}{\Delta\omega_r - \Delta\hat{\omega}_r} = \frac{\left(s + \frac{1}{\tau_r}\right)|\boldsymbol{\lambda}_r|^2}{\left(s + \frac{1}{\tau_r}\right)^2 + \omega_s^2}. \tag{6}$$

Fig. 2 depicts the whole block diagram from the proposed speed estimation

B. Pole Assignment of the Speed Estimator

Assuming that $\omega_s = 0$ for simplicity, we can specify the damping factor ξ and natural angular frequency ω_c by using K_P and K_I in (4) as follows:

$$\begin{cases} K_P = (2\xi\omega_c - 1/\tau_r)/|\boldsymbol{\lambda}_r|^2 \\ K_I = \omega_c^2/|\boldsymbol{\lambda}_r|^2. \end{cases} \tag{7}$$

From (7), the transfer function from $\Delta\omega_r$ to $\Delta\hat{\omega}_r$ is

$$\frac{\Delta\hat{\omega}_r}{\Delta\omega_r} = \frac{(2\xi\omega_c - 1/\tau_r)s + \omega_c^2}{s^2 + 2\xi\omega_c s + \omega_c^2}. \tag{8}$$

We can see that the speed estimation dynamics are characterized by one zero and two poles given by

$$\begin{cases} \text{zero: } s_z = -\dfrac{\omega_c^2}{2\xi\omega_c - 1/\tau_r}. \\ \text{poles: } s_p = -\xi\omega_c \pm j\omega_c\sqrt{1-\xi^2}. \end{cases} \tag{9}$$

IV. Flux Observer

A. Basic Design of the Flux Observer

We designed another flux observer to be used for field-orientation control by using Gopinath's reduced order observer theory, which we proposed previously [5].

The observer equation takes the form of

$$\begin{aligned} \dot{\hat{\boldsymbol{\lambda}}} &= \boldsymbol{A}_{22}\hat{\boldsymbol{\lambda}}_r + \boldsymbol{A}_{21}\boldsymbol{i}_s + \boldsymbol{G}(\dot{\boldsymbol{i}}_s - \boldsymbol{A}_{12}\hat{\boldsymbol{\lambda}}_r - \boldsymbol{A}_{11}\boldsymbol{i}_s - \boldsymbol{B}_1\boldsymbol{v}_s) \\ &= -\boldsymbol{H}\hat{\boldsymbol{\lambda}}_r + (\boldsymbol{A}_{21} - \boldsymbol{G}\boldsymbol{A}_{11})\boldsymbol{i}_s - \boldsymbol{G}\boldsymbol{B}_1\boldsymbol{v}_s + \boldsymbol{G}\dot{\boldsymbol{i}}_s. \end{aligned} \tag{10}$$

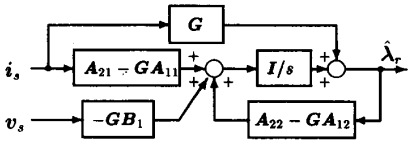

Fig. 3. Configuration of flux observer.

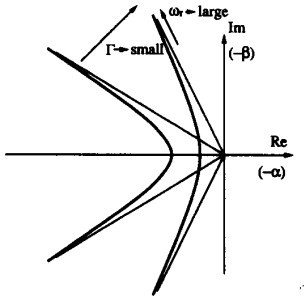

Fig. 4. Pole allocation of the flux observer.

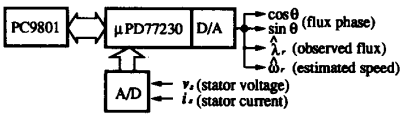

Fig. 5. Setup of the experimental system centered about DSP.

In the case of no parameter variations, the dynamics of the flux estimation error $\boldsymbol{e} = \hat{\boldsymbol{\lambda}}_r - \boldsymbol{\lambda}_r$ takes the form of

$$\dot{\boldsymbol{e}} = (\boldsymbol{A}_{22} - \boldsymbol{G}\boldsymbol{A}_{12})\boldsymbol{e} = -\boldsymbol{H}\boldsymbol{e}. \tag{11}$$

The eigenvalues of $-\boldsymbol{H}$ are the observer poles, which can be specified freely by the observer gain $\boldsymbol{G}$ because this system satisfies the observability condition.

Fig. 3 depicts the configuration of our flux observer.

B. Pole Allocation that realizes the Robust Flux Observer

We investigated the case where only R_r is different from its nominal value used in the observer. When $'$ is attached to the actual values as

$$\boldsymbol{A}'_{ij} = \boldsymbol{A}_{ij} + \Delta\boldsymbol{A}_{ij} \tag{12}$$

the error function (11) comes to have additional terms as given by

$$\dot{\boldsymbol{e}} = -\boldsymbol{H}\boldsymbol{e} + \boldsymbol{H}\boldsymbol{A}_{12}^{-1}(\Delta\boldsymbol{A}_{12}\boldsymbol{\lambda}_r + \Delta\boldsymbol{A}_{11}\boldsymbol{i}_s). \tag{13}$$

From (13), we can notice that the matrix norm $\|\boldsymbol{H}\boldsymbol{A}_{12}^{-1}\|_2$ represents the sensitivity of the observer to R_r variation.

By solving a kind of optimal control problem for the error system, we specified the observer poles $-\alpha \pm j\beta$ by

$$\begin{cases} \alpha = \sqrt{1/\tau_r^2 + \Gamma^2(1/\tau_r^2 + \omega_r^2)} \\ \beta = -\omega_r. \end{cases} \tag{14}$$

This pole allocation keeps the norm $\|\boldsymbol{H}\boldsymbol{A}_{12}^{-1}\|_2$ to be constant regardless of the motor speed as

$$\|\boldsymbol{H}\boldsymbol{A}_{12}^{-1}S\|_2 = \frac{\sqrt{1+\Gamma^2}}{\kappa}. \tag{15}$$

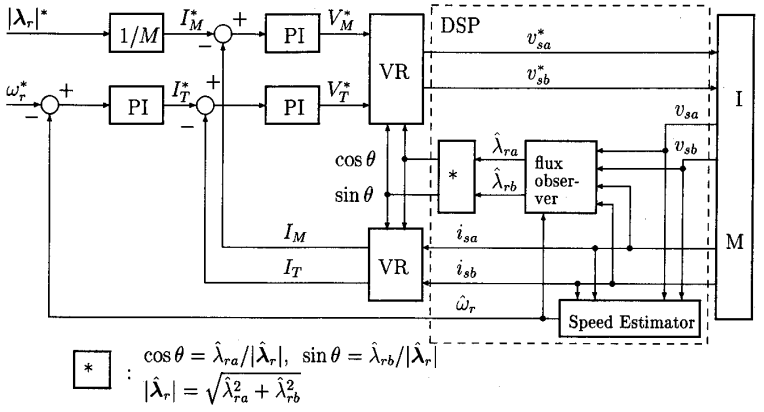

Fig. 6. Speed-sensorless field-orientation control system.

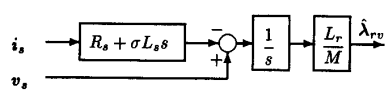

Fig. 7. Voltage model.

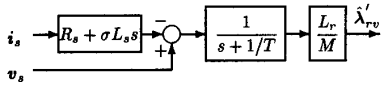

Fig. 8. Modified voltage model.

This was the key of our success in the realization of FOFO control system [5]. Fig. 4 shows that the observer poles move according to the motor speed ω_r. Γ is the only parameter in our pole allocation. In the following experiments, we used $\Gamma = 1.0$.

V. Experimental Results

A. Experimental Setup

Fig. 5 shows the DSP-based implementation of the speed-sensorless FOFO controller. The DSP used was the μPD77 230 made by NEC, which can perform 32-b floating-point multiplication. Its clock frequency is 13.333 MHz, and the machine cycle for every calculation is 150 ns.

The tested machine is a four-pole 2.2-kW induction machine that has the following parameters:

$$\begin{cases} R_s = 0.877\,\Omega & R_r = 1.47\,\Omega \\ L_s = 165.142\,\text{mH} & L_r = 165.142\,\text{mH} \\ M = 160.8\,\text{mH} & \sigma = 0.0519. \end{cases}$$

Fig. 6 shows the block diagram of the speed-sensorless field-orientation control system. The speed estimator calculates the speed $\hat{\omega}_r$ from the stator voltage and current components, and this estimated speed is immediately used for the flux observer and the speed controller.

The DSP performs the calculations required for the speed estimator and the flux observer (inside the dashed lines).

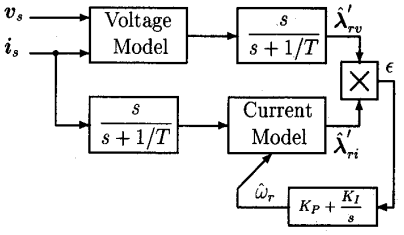

Fig. 9. Speed estimator (experiment).

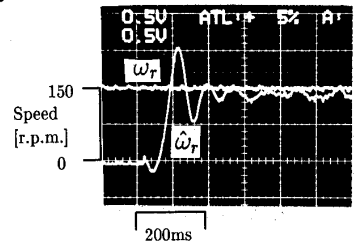

(a)

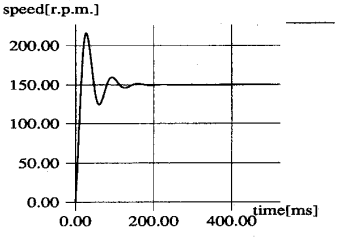

(b)

Fig. 10. Dynamic response of speed estimator ($\xi = 0.29$, $\omega_c = 100$): (a) Experimental result; (b) calculation result.

B. Some Modification in Actual Speed Estimator

In practice, the original voltage model of (2) is difficult to implement because it requires a pure integrator, which has the initial value and drift problems. To avoid these problems we replaced the pure integrator by the low-pass filter. This

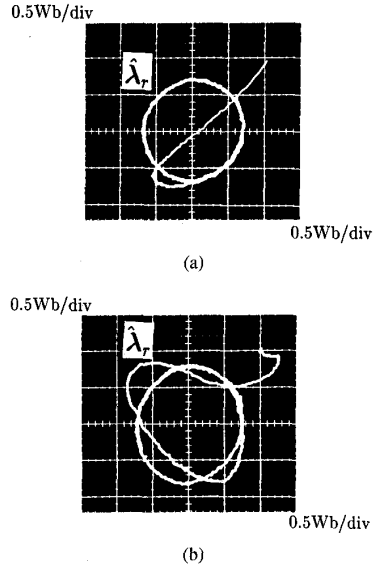

Fig. 11. Flux observation: (a) Using measured speed ω_r; (b) using estimated speed $\hat{\omega}_r$.

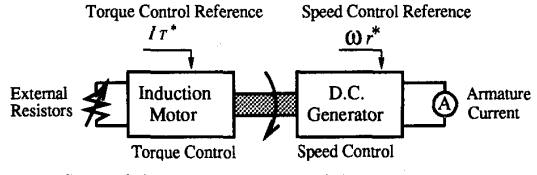

Fig. 12. Setup of the measuring system of the stationary torque errors to changes in the rotor resistance.

modified voltage model has the form of

$$\dot{\hat{\lambda}}'_{rv} = -\frac{1}{T}\hat{\lambda}'_{rv} + \frac{L_r}{M}(\boldsymbol{v}_s - R_s\boldsymbol{i}_s - \sigma L_s\dot{\boldsymbol{i}}_s). \qquad (16)$$

The voltage model and the modified voltage model are illustrated in Fig. 7 and 8, respectively. Since the output of the modified voltage model of (16) is different from the rotor flux, we have to modify the current model simultaneously. The modified voltage in Fig. 8 is equivalent to one that consists of a voltage model and a high-pass filter (HPF). Hence, the modification of the current model is achieved by inserting HPF (see Fig. 9). T is a time constant of HPF. In the experiment, we use $T = 0.05$; then, its cut-off frequency is about 3.2 Hz.

C. Experimental Results of Speed Estimation

Fig. 10 shows the speed estimation performances. Fig. 10(a) is the experimental result of Fig. 9, and (b) is the result calculated by linear model of (8). In case of $\xi = 1.0, \omega_c = 100$, PI parameters are obtained as $K_P = 399$, $K_I = 20\,408$ from (7). However, when we use these PI parameters, the estimated speed becomes very noisy because the proportional gain K_P may be too large. Then, we used smaller proportional gain $K_P = 100$. It is equivalent to the case of $\xi = 0.29$ and $\omega_c = 100$. This choice means that the convergence has a fairly oscillational damping characteristics.

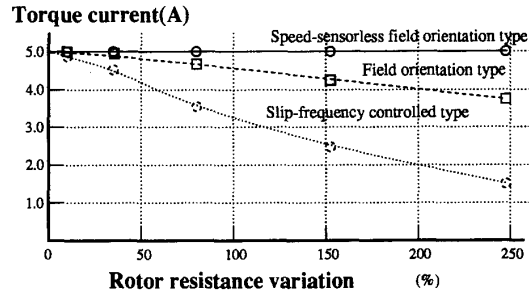

Fig. 13. Stationary torque errors caused by R_r variation ($\omega_r = 75$ r/min).

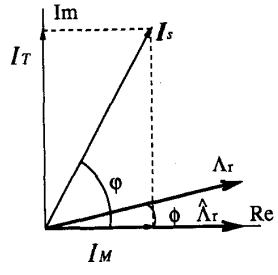

Fig. 14. Vector diagram of flux and current.

The agreement of Fig. 10(a) and (b) is not very good because the linear model (8) is the reduced model that ignores HPF and the slip. The estimated speed dynamics has an oscillational damping. Hence, we can say that the speed can be estimated effectively with the convergence characteristics specified by ξ and ω_c.

The MRAS speed estimator does never work by arbitrary K_P and K_I parameters. We than proposed a novel method to determine PI parameters by (7) and adjusted the parameters by the experiment.

D. Experimental Results of Flux Estimation

The estimated speed is used in the flux observer as an important parameter of matrices in (10). Fig. 11 shows the flux estimation convergence performances of the flux observers from initial value ($\hat{\lambda}_{r0}$ =(1.0 Wb, 1.0 Wb)), where (a) is the case of using the measured speed ω_r and (b) is the case of using the estimated speed ω_r, respectively. (b) has a transient dynamics in convergence from initial value, but once the estimated flux converges, the estimation performance is good in both cases.

E. Robustness of Torque Control to the Machine Parameter Variation

Fig. 13 shows the stationary torque errors caused by the variation of rotor resistance R_r. The tested induction machine is connected to a dc generator, and the induction machine commands the generation of constant torque. The rotation is maintained at a constant speed by the load dc machine (see Fig. 12). We can see that the proposed field-orientation controller using the estimated speed (it is noted "speed-sensorless field orientation type") is completely insensitive to R_r variation.

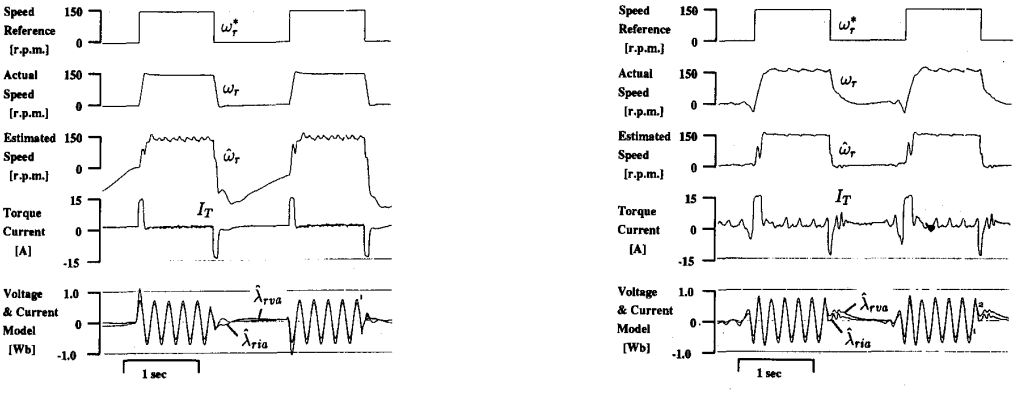

Fig. 15. Speed control response (0↔150 r/min): (a) Using measured speed; (b) using estimated speed.

This can be explained as follows. The flux observer (10) has a skew-symmetric structure; therefore, we can interpret its diagonal parts as the real parts and the skew symmetric parts as imaginary parts of the complex number as follows

$$\begin{cases} \boldsymbol{\Lambda}_r = \Lambda_{ra} + j\Lambda_{rb} \\ \hat{\boldsymbol{\Lambda}}_r = \hat{\Lambda}_{ra} + j\hat{\Lambda}_{rb} \end{cases} \tag{17}$$

where $\boldsymbol{\Lambda}_r$ is the real flux, and $\hat{\boldsymbol{\Lambda}}_r$ is the observed flux in steady state, respectively.

The steady-state error of the estimated flux can be calculated using (10) and (17). When the rotor resistance varies and we use the estimated speed for the flux observer, it takes the form of

$$\frac{\hat{\boldsymbol{\Lambda}}_r - \boldsymbol{\Lambda}_r}{\boldsymbol{\Lambda}_r} = \frac{\alpha - j\omega_r}{\alpha + j\omega_s} \frac{-j}{(1/\tau_r - j\omega_r)} \cdot \left(\omega_s \frac{\Delta R_r}{R_r'} - \Delta\omega_r \right) \tag{18}$$

where

$$\begin{cases} \Delta R_r = R_r' - R_r \\ \Delta\omega_r = \hat{\omega}_r - \omega_r. \end{cases} \tag{19}$$

R_r' is the actual rotor resistance. $\Delta\omega_r$, which is the estimation error of the speed, can be calculated using (3). It is given by

$$\Delta\omega_r = \omega_s \frac{\Delta R_r}{R_r'}. \tag{20}$$

Fig. 14 depicts the vector diagram of flux and current. Under field-orientation control, the stationary torque error is given by

$$\frac{T}{T^*} = \left| \frac{\boldsymbol{\Lambda}_r}{\hat{\boldsymbol{\Lambda}}_r} \right| \frac{\sin(\varphi - \phi)}{\sin\varphi} \tag{21}$$

where T^* is torque reference, and T is actual torque, respectively.

Equations (18) and (20) tell us that the flux estimation error is zero. This means that the angle ϕ in Fig. 14 is zero. Then from (21) we can notice that the stationary torque is insensitive to R_r variation.

F. Speed Control Response

Figs. 15 and 16 show the speed control responses, where (a) in each is of the slip frequency controller using the measured speed ω_r, and (b) is of the speed sensorless FOFO controller using the estimated speed $\hat{\omega}_r$. The waveforms are speed reference (ω_r^*), actual speed (ω_r), estimated speed ($\hat{\omega}_r$), and flux simulator output ($\hat{\lambda}_{rva}$, $\hat{\lambda}_{ria}$), respectively. Speed reference was a 0.5 Hz rectangular waveform of $0 \sim 150$ r/min (Fig. 15) and $-150 \sim 150$ r/min (Fig. 16).

The estimated speed in Figs. 15(a) and 16(a) are calculated but not used for speed control. The estimated speed is in good agreement with the actual speed in the higher speeds, but in the lower speed region, the estimated speed has a considerable transient error. It is caused by HPF used in the speed estimator (see Fig. 9). Due to the presence of HPF, the flux simulator output signal at low frequency is highly attenuated, and therefore, speed estimation performance is poor.

In contrast, in Figs. 15(b) and 16(b), the estimated speed is immediately used for speed controller feedback signal and for the flux observer. The estimated speed corresponds with the actual speed even at lower speed range, and the speed itself can be controlled fairly well. Estimated spread feedback causes torque current to increase. This in turn, causes a proportional increase in slip frequency and source frequency, causing the flux simulator output to improve.

VI. Conclusion

We proposed the speed sensorless FOFO controller for the induction machine. The motor speed is estimated based on the difference between the outputs of two flux simulators. The torque generated by the system is extremely robust to rotor resistance variations. We implemented the system using a DSP and showed its efficacy through laboratory experiments.

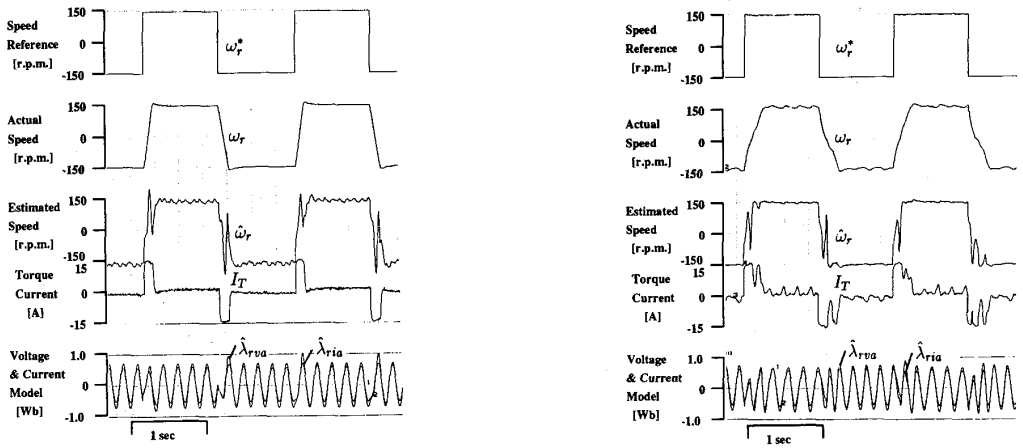

Fig. 16. Speed control response ($-150 \rightarrow 150$ r/min): (a) Using measured speed; (b) using estimated speed.

ACKNOWLEDGMENT

The authors would like to express their acknowledgment to Prof. Y. Kaya for his guidance and all kinds of wise advice.

REFERENCES

[1] C. Schauder, "Adaptive speed identification for vector control of induction motors without rotational transducers," in *Proc. 1989 IAS Ann. Mtg.* (San Diego), pp. 493–499.
[2] T. Ohtani, N. Takada, and K. Tanaka, "Vector control of induction motor without shaft encoder," in *Proc. 1989 IAS Ann. Mtg.* (San Diego), pp. 500–507.
[3] G. C. Verghese *et al.*, "Observers for flux estimation in induction machines," *IEEE Trans. Ind. Electron.*, vol. 35, no. 1, 1988.
[4] Y. Hori, V. Cotter, and Y. Kaya, "A novel induction machine flux observer and its application to a high performance ac drive system," in *Proc. IFAC '87*, pp. 355–360.
[5] Y. Hori and T. Umeno, "Implementation of robust flux observer based field orientation controller for induction machines," in *Proc. 1989 IAS Ann. Mtg.* (San Diego), pp. 523–528.
[6] I. Miyashita and Y. Ohmori, "Speed sensorless high-speed torque and speed control based on instantaneous spatial vector theory," in *Proc. IPEC-Tokyo '90*, pp. 1144–1151.
[7] X. Xu and D. W. Novotny, "Implementation of direct stator flux orientation control on a versatile DSP based system," *Proc. 1990 IAS Ann. Mgt.* (Seattle), pp. 404–409.
[8] M. Vélez-Reyes, K. Minami, and G. C. Verghese,"Recursive speed and parameter estimation for induction machines," in *Proc. 1989 IAS Ann. Mtg.* (San Diego), pp. 607–611.
[9] U. Baader, M. Depenbrock, and G. Gierse, "Direct self control of inverter-fed induction machine; A basis for speed control without speed-measurement," in *Proc. 1989 IAS Ann. Mtg.* (San Diego), pp. 486–492.

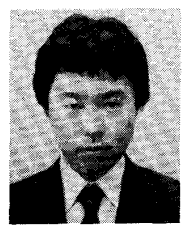

Hirokazu Tajima was born in Tokyo, Japan, on July 12, 1967. He received the B.E. and M.E. degrees in electrical engineering from the University of Tokyo, Tokyo, Japan, in 1990 and 1992, respectively.

Since Apr. 1992, he has been with Fuji Electric Corporate Research and Development, Ltd. His research interests are in control theory and its application to motor drives.

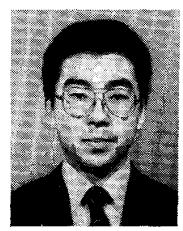

Yoichi Hori (M'83) received the B.Sc., M.Sc., and Ph.D. degrees in electrical engineering from the University of Tokyo, Tokyo, Japan, in 1978, 1980 and 1983, respectively.

He is now an Associate Professor in the Department of Electrical Engineering, University of Tokyo. His research interests are in control theory and its application to robotics, mechatronics, and power electronics.